ChemComm

Accepted Manuscript

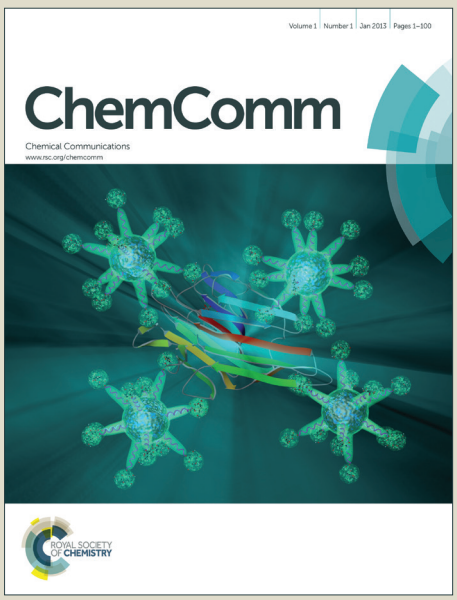

ROYAL SOCIETY OF CHEMISTRY

www.rsc.org/chemcomm

Journal Name

RSCPublishing

COMMUNICATION

Crystallization of rubrene on nanopillar-templated surface by melt-process and its application in field-effect transistors

Cite this: DOI: 10.1039/x0xx00000x

Received 00th January 2012,
Accepted 00th January 2012

DOI: 10.1039/x0xx00000x

www.rsc.org/

Chi-Chih Ho[a,b,c] and Yu-Tai Tao[a,*]

a. Institute of Chemistry, Academia Sinica, Taipei, Taiwan
b. Nano Science and Technology Program, Taiwan International Graduate Program, Academia Sinica, Taipei, Taiwan and National Tsing Hua University, Hsinchu, Taiwan
c. Department of Engineering and System Science, National Tsing Hua University, Hsinchu, Taiwan

We present an approach to fabricate a continuous and crystalline rubrene film using melt-recrystallization process with the assistance of a silicon nanopillar template. Better film morphology, enhanced crystallinity, and mainly oriented crystallites with c-axis of the orthorhombic rubrene aligning parallel to the nanopillars were obtained as compared to that on a planar substrate. The oriented crystal growth is further modulated by the surface modification. It is suggested that the sidewalls of nanopillars play a key role in mediating the switch of crystal orientation and crystal growth. The obtained nanopillar-templated rubrene film was used to fabricate a vertical field-effect transistor. The device gave a current density of 78 mA/cm^2, on-off ratio around 10^{3-4}, subthreshold swing of 89.1 mV/decade and transconductance of 154.9 mS/cm^2 on ODTS-modified substrate surface.

Organic field-effect transistors (OFETs) are expected to be one of the essential components in building printable, flexible and cost-effective micro/nano electronics. The organic semiconducting layers used in these devices are often prepared by vacuum deposition,[1] physical vapour transport (PVT)[2] or solution processes[3]. Among them, solution processes are favoured for scalable manufacturing because it is not limited to the size of substrates, volatility of the materials and the immethodical crystal growth from PVT. Common solution processing techniques include spin-coating, doctor blading, inkjet printing and dip coating, each involves rather cheap and simple fabricating processes.[4] On the other hand, the charge transporting property is highly sensitive to the crystallinity and morphology of the semiconducting film.[5] To obtain a crystalline layer with an uninterrupted coverage over a substrate directly from solution process remains challenging.

Controlling of crystal growth habit and morphology has been the focus of research efforts for solution-processed films. For example, flow shearing with a micropillar-patterned blade was used to align crystal domains to a preferred orientation and the deposited TIPS-pentacene thin film displays a large charge mobility of 11 cm^2/Vs.[6] Other examples of influencing crystallinity are adding nucleating agent,[7] roughening the surface[8] or providing vitreous environment[9] to the main semiconducting materials for improved heterogeneous nucleation. In terms of morphology, polymers can easily achieve a continuous and flat film from solution process with their crystalline domains bridged by macromolecular chains. However, small semiconducting molecules lacking chain entanglements normally form separated droplets or islands/patches during drying or annealing process. These defects result in morphological imperfections and become the obstacle for extensive use. To reduce these defects, further surface modification on substrate,[10] aided *via* polymer hybrids[11] or the control of convective flow[12] has been reported as effective routes.

Rubrene is a well-known and readily available semiconductor molecule, giving one of the highest field-effect mobility (20 cm^2/Vs) in the single crystal state.[2] It is nevertheless also known that crystalline rubrene film can hardly be prepared by simple vapour evaporation on clean wafer surface (mobility~10^{-6} cm^2/Vs) [13]. An enhanced crystallinity of evaporated rubrene was found on a surface with large molecular steps purposely constructed by thick self-assembled multilayers[14] or pentacene-buffered layer.[15] These results may imply, among other possibilities, that the sidewalls from nanostructures may help the crystal growth. In this paper, we present a simple melt process to manipulate both crystallinity and morphology of films of rubrene molecules as assisted by a nanopillar-templated substrate and surface modification. The scheme in Figure 1 shows our newly developed process, which mainly relies on two strategies. Firstly, the capillary filling, created by the nanopillar arrays, regulates the molten rubrene to a continuous film. Secondly, the sidewalls of nanopillars provide large amount of surface area as preferred sites for heterogeneous nucleation during melt-recrystallization process. The resulting rubrene film is continuous and exhibits crystalline domains with preferred orientation. A high transconductance and current density were achieved under a vertical transistor configuration, which enables the operation of an OLED pixel. The simple methodology may provide an alternative to those nanoelectronics requiring vertical conducting channel configuration.

The rubrene was dissolved in toluene to saturation. The solution was spread on a silicon nanopillar template, which was prepared according to a literature protocol.[16] The wafer-scaled nanopillar arrays have adjustable dimensions in the height (500 nm to 2μm),

diameter (600 nm to 300 nm) and period (780 nm to1000 nm). After solvent evaporation, the substrate, originally kept at 90 ˚C, was heated up to the melting temperature of rubrene under nitrogen atmosphere. The molten rubrene filled into the spaces between nanopillars immediately. Upon normal cooling, the rubrene solidified and was molded by the nanopillar template. The cartoons in Figure 1 schematically show the fabricating process.

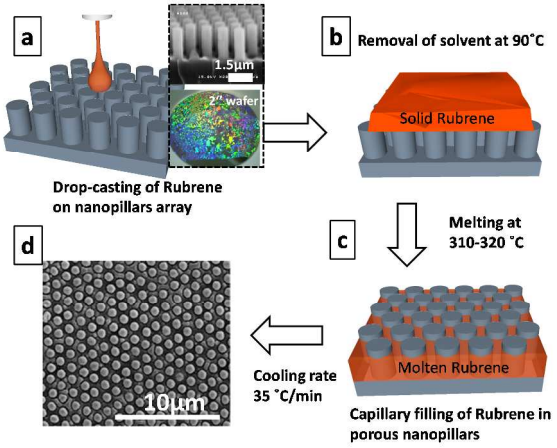

Fig.1 A schematic illustration. (a) Drop-casting of rubrene solution on nanopillar template; (b) Removal of solvent at 90˚C, leaving solid on the surface; (c) An abrupt heating to 320˚C to reach melting. About 1.5 -2 minutes for implanting the molten rubrene into spaces between nanopillars. (d) Normal cooling to 180˚C and annealing at 180˚C for 30 minutes before further cooling to room temperature.

The melt-processed rubrene on nanopillar-templated surface has morphologies significantly different from that prepared on a planar surface. On a planar surface, discrete droplets are normally formed because the surface tension of rubrene outweighs the wetting (spreading) tendency, as shown in Figure 2a. This is true for piranha-cleaned and unmodified silicon wafer surface as well surfaces modified with self-assembled monolayer (SAM) of octadecyltrichlorosilane (ODTS), octyltrichlorosilane (OTS) or 1H,1H,2H,2H-Perfluorooctyltrichlorosilane (FOTS). Presumably these SAM modifications further reduce the surface energy and decrease the wettability of the surface. In contrast, the nanopillar arrays allow the molten rubrene to flow into the spaces between pillars and laterally spread over a large area. The capillary forces exerted from periodic nanopillars guide the liquid to form a continuous film. The uniformity is presented in Figure 2b, where the green dots and red networks are the locations of nanopillars and the rubrene film respectively.

Further details of film morphology of recrystallized rubrene on planar and nanopillar surfaces are provided by scanning electron microscopy (SEM), as shown in Figure 2c and 2d. A noteworthy feature observed in nanopillar-templated rubrene is that, the columnar-like rubrene crystals grew against substrate with their long-axes near parallel to nanopillars. The x-ray diffraction (XRD) measurements were carried out to reveal the crystallinity and phase of the rubrene films. The XRD observations in Figure 3a suggest poor crystallinity for those rounded solids formed on a planar surface[13] and relatively high degree of crystallinity for the rubrene prepared on nanopillar-templated surface. For a fair comparison, equal amount of rubrene was spread on the same sample area.

The peak positions/intensities reveal information on the crystal phase and orientation. Rubrene commonly crystalizes into three kinds of phases (monoclinic, triclinic and orthorhombic). For the rubrene recrystallized on a planar wafer, a sole peak was observed at $2\theta = 6.61^{\circ}$ on each SAM-modified surface (Figure 3a). The peak position coincides with the (200) peak for orthorhombic rubrene (a = 26.9 Å).

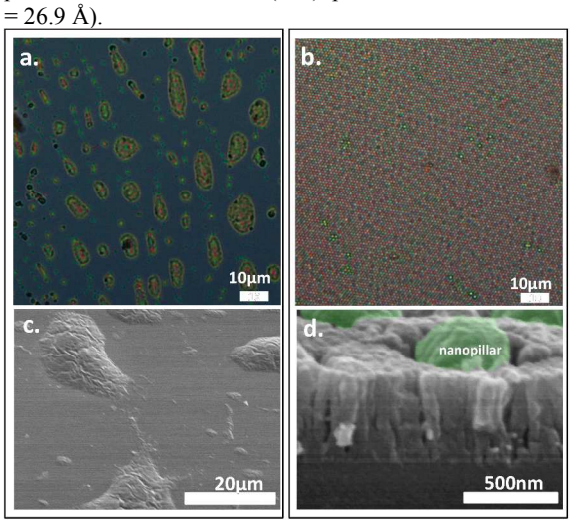

Fig. 2 A comparison between optical images of rubrene recrystallized on (a) piranha-cleaned Si wafer, and (b) nanopillar-templated surface. (c) and (d) are the SEM images of bird-eye-view and cross sectional view of (a) and (b). The oriented nanocrystals are easily seen in (d). The locations of nanopillars are marked in green.

Thus the rubrene droplets on a planar wafer have their crystallized parts oriented in such a way that their a-axis aligned perpendicular to the substrate. For rubrene recrystallized on the nanopillar-template, a second strong peak at $2\theta = 12.25^{\circ}$ was found in each system.

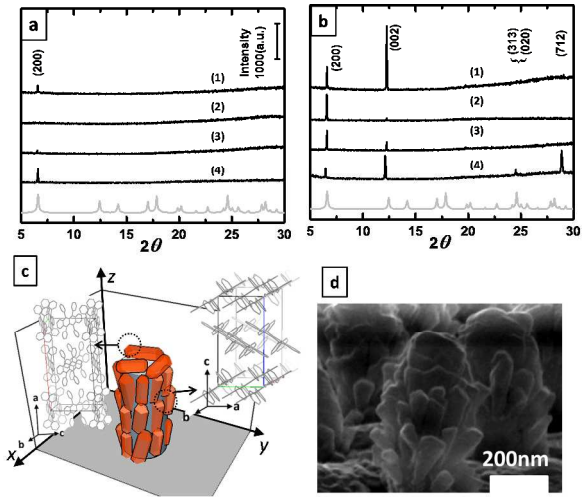

Fig. 3 The XRD for rubrene on substrates with different SAM modifications: ODTS (curve 1), FOTS (curve 2), OTS (curve 3) and piranha-cleaned Si (curve 4), for (a) planar substrate (b) nanopillar template, compared with the calculated XRD of orthorhombic powders (grey curve).[17] (c) A 3D sketch of crystals orientation and distribution (d) corresponding cross-sectional SEM image for a rubrene sample not fully covering the nanopillars.

This peak was assigned as (002) diffraction (c = 14.4 Å) of orthorhombic rubrene. The SEM image for a rubrene sample with nanopillars partly covered (using insufficient amount of rubrene, Figure 3d) can help to understand the appearance of (002) diffractive peak. As mentioned earlier, columns of rubrene crystal were formed around the nanopillars with the long crystal axes aligned nearly

parallel to the pillars. It is suggested that this is the c-axes of the crystals so that the a-axes aligned normal to the pillar surface, in agreement with the observation that rubrene crystals tend to grow so that their a-axes are perpendicular to the substrate surface, only that now the surface is that of the sidewalls of the nanopillars. The co-existence of (002) peak and (200) peak implies there are also crystals influenced by the bottom surfaces between the pillars and/or the top of pillars,[18] as sketched in 3-dimension in Figure 3c. The relative intensities of the two and thus the amount of the two may also relate to the surface modification. Thus for the ODTS-modified nanopillar surface, there was a predominance of crystals having their c-axes aligning along the nanopillars by comparing the intensity ratios of the two peaks $I_{(002)}/I_{(200)}$. Yet on FOTS-modified surface, there was least amount of crystals with c-axes aligning along nanopillars. The effect of different SAMs is believed to be the wetting property and thus the sticking ability of the molecules at the surface. FOTS-modified surface is of lowest surface energy and least sticky. The ODTS(C18)-modified and OTS(C8)-modified surfaces are different presumably because the C18 monolayer is more ordered and solid-like and C8 monolayer is disordered and liquid-like. These differences will also influence the directing effect of the sidewalls.

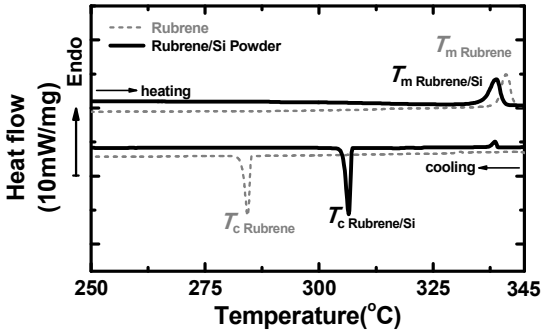

Fig. 4 DSC analyses of rubrene powders. The grey dashed line is the heating and cooling curves of pure rubrene at a rate of 10˚C/min. The solid line is the grind mixture of rubrene and ODTS-modified silicon powder. The T_c and T_m denote the recrystallization and melting temperatures respectively.

The recrystallization from melt occurs by nucleation and growth during a given temperature gradient. In most cases, the homogeneous nucleation is a rather difficult process and often requires high degree of supercooling to induce critical-sized embryo. As a test, the differential scanning calorimetry (DSC) measurement of pure rubrene and a grind mixture of micrometer-sized silicon powder (1:1 by weight, a simulation of the environment for the rubrene surrounded by nanopillar sidewalls) was carried out. As shown in Figure 4, the grey dashed traces refer to the heating and cooling curves of pure rubrene at a rate of 10˚C/min. A clear exothermal peak of recrystallization was observed at 284˚C, while the melting occurred at 337 ˚C. On the other hand, the grind mixture of solid rubrene and silicon powder gave the solid line in Figure 4, where the exothermal peak of recrystallization was observed at 306 ˚C. The recrystallization temperature in rubrene/Si powder mixture occurred about 22 ˚C earlier than that for pure rubrene. This indirectly supports the suggestion of enhanced heterogeneous nucleation from the sidewalls of porous nanopillars.[19] It is suggested that the better crystallinity on nanopillar-templated substrate results from the easier nucleation process compared to nucleating homogeneously. In the case of planar surface, much of the bulk volume of the rubrene liquid are far away from the substrate surface and may solidify directly to amorphous phase.

With crystals mainly aligned along the sidewall of nanopillars, charge transport along this direction, as required in the vertical transistors, is of interest. The crystallized rubrene films templated by nanopillars were used to fabricate vertical organic FETs (VOFET). The layout, energy band diagram and geometry of the VOFET are shown in Figure 5a, 5b and 5c, respectively, with a vertical channel length L = 440 nm, periodicity p = 1000 nm and diameter D = 385 nm. Metal source/drain electrodes (Cr/Au = 3/60 nm and Al = 200 nm) were deposited at the device bottom and top of the nanopillars by thermal evaporation. The silicon pillars served as gate with thermally-grown oxides (90 nm) on the surface as dielectric layer. A SiO_x hat was made on each nanopillar top by evaporation on a tilted and rotating substrate to prevent the gold clusters from attaching to the sidewalls while depositing source electrode.

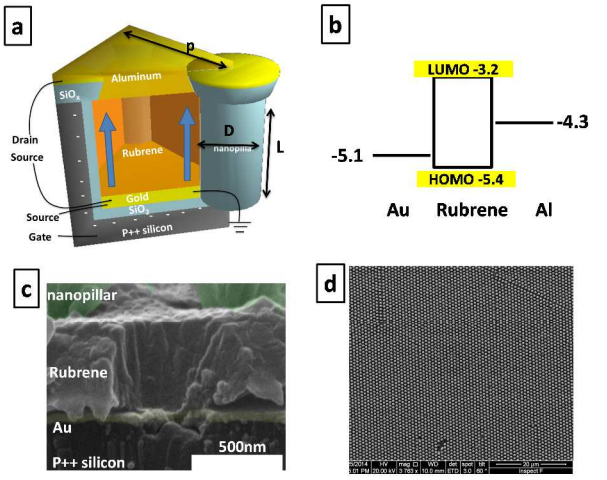

Fig. 5 VOFET device: (a) the 3D layout; (b) energy band diagram; (c) cross-sectional SEM image, and (d) top-view. The position of nanopillars and gold electrode are painted as green and yellow by pseudo colour in (c), with the "hole" as the position of a pillar that was ripped off by the cutting process.

Figure 6a shows the transfer characteristic (J_{DS} vs. V_G) of the VOFET, displaying a threshold voltage of approximately 1.3 V, with a current density of 78 mA/cm^2 at gate bias < -1 V, and a subthreshold swing (SS) of 89.1 mV/decade as suggested in the inset. The very similar device performances of low operating voltage and high output current have been previously reported in other OFETs with vertical configuration.[20] The I_{DS}-V_{DS} characteristics at various gate biases are shown in Figure 6, where no saturation region was observed. At zero gate bias, the I_{DS}-V_{DS} in the log-log scale plot shows a slop of ~2.1, agreeing with the requirement for the power relation of $I_{DS} \propto V^{n}_{DS}$ $(n \geq 2)$ [21] for devices operating with space-charge-limited current. Indeed, with our device configuration with a vertical channel length less than 1μm is simply a metal-organic-metal diode. However, with negative bias applied at the gate, the current enhanced and the slope n decreased, as shown in the inset of Figure 6b. This may suggest the current contribution from gate-induced carriers near the pillar surfaces. Absence of saturation regime can be due to short channel effect.[22] Thus the charge transport mechanism may contain both bulk current and surface current, depending on the applied negative potential on nanopillar sidewalls. Here, we evaluated the performance through the transconductance per unit area ($g_m = \partial J_{DS} / \partial V_G$). The g_m is estimated to be 154.9 mS/cm^2, which is about 3-fold larger than a previous vertical transistor using low-mobility material.[20d] The large

transconductance in the present device can be associated with the oriented growth of rubrene crystallites induced by the nanopillars and the fine field-effect mobility for hole carriers transporting along c-axes in orthorhombic rubrene.[23] In contrast, the transconductance for rubrene films obtained on FOTS-modified substrate was calculated to be 4.43 mS/cm^2. That for samples with bare silicon surface and OTS-modified substrate were not measurable. For reference, conventional FET device made with this rubrene film gave rather poor mobility of 0.0042 cm^2/Vs.[24]

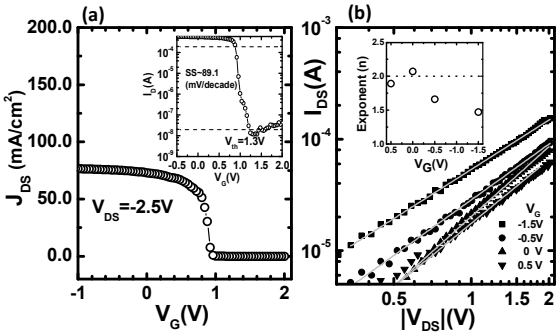

Fig. 6 (a) The transfer characteristics of VOFET. (b) A log-log plot of I_{DS}-V_{DS} at various V_G for extracting the exponents. The grey lines are the linearly fitted curves to reveal the slopes. The inset shows a decreasing trend of n as a function of V_G.

Conclusions

In summary, we demonstrated a simple melt process to prepare crystalline films of rubrene using a nanopillars array. The resulted film is continuous, and has preferred orientation in the crystal growth. The main mechanisms comprise capillary filling, melt-recrystallizing process and enhanced heterogeneous nucleation. The crystal domains were found to collectively align in a manner such that their c-axes are nearly parallel to the nanopillars. The oriented crystalline film was utilized to fabricate field-effect transistor in a vertical configuration, with the nanopillars as the gate electrode. The device shows very promising performance characteristics, having threshold voltage of 1.3 V, areal current density of 78 mA/cm^2, on-off ratio of 10^{3-4}, subthreshold swing of 89.1 mV/decade and a high transconductance of 154.9 mS/cm^2. We also suggest that charge carriers transport in the bulk due to space-charge limited transport, as well as near the nanopillar surface due to the charge carriers from the gate effect. The ordered nanopillar architecture incorporated here may not only serve as nucleating agent but also as functional elements. We anticipate a more general application for a uniform organic crystal/nanopillar hybrid system in functional nanoelectronics.

Notes and references

* ytt@gate.sinica.edu.tw

1. Nelson, S. F.; Lin, Y.-Y.; Gundlach, D. J.; Jackson, T. N., *Applied Physics Letters* 1998, **72**, 1854-1856.
2. Podzorov, V.; Menard, E.; Borissov, A.; Kiryukhin, V.; Rogers, J. A.; Gershenson, M. E., *Physical Review Letters* 2004, **93**, 086602.
3. Sirringhaus, H., *Advanced Materials* 2005, **17**, 2411-2425.
4. Wen, Y.; Liu, Y.; Guo, Y.; Yu, G.; Hu, W., *Chemical Reviews* 2011, **111**, 3358-3406.
5. Wang, C.; Dong, H.; Hu, W.; Liu, Y.; Zhu, D., *Chemical Reviews* 2011, **112**, 2208-2267.
6. Diao, Y.; Tee, B. C. K.; Giri, G.; Xu, J.; Kim, D. H.; Becerril, H. A.; Stoltenberg, R. M.; Lee, T. H.; Xue, G.; Mannsfeld, S. C. B.; Bao, Z., *Nat Mater* 2013, **12**, 665-671.
7. Treat, N. D.; Nekuda Malik, J. A.; Reid, O.; Yu, L.; Shuttle, C. G.; Rumbles, G.; Hawker, C. J.; Chabinyc, M. L.; Smith, P.; Stingelin, N., *Nat Mater* 2013, **12**, 628-633.
8. Di, C.-a.; Liu, Y.; Yu, G.; Zhu, D., *Accounts of Chemical Research* 2009, **42**, 1573-1583.
9. Stingelin-Stutzmann, N.; Smits, E.; Wondergem, H.; Tanase, C.; Blom, P.; Smith, P.; de Leeuw, D., *Nat Mater* 2005, **4**, 601-606.
10. Kim, Y.-H.; Yoo, B.; Anthony, J. E.; Park, S. K., *Advanced Materials* 2012, **24**, 497-502.
11. Su, Y.; Liu, J.; Zheng, L.; Ding, Z.; Han, Y., *RSC Advances* 2012, **2**, 5779-5788.
12. Lim, J. A.; Lee, W. H.; Lee, H. S.; Lee, J. H.; Park, Y. D.; Cho, K., *Advanced Functional Materials* 2008, **18**, 229-234.
13. Seo, S.; Park, B.-N.; Evans, P. G., *Applied Physics Letters* 2006, **88**, 232114.
14. Wang, C.-H.; Islam, A. K. M. M.; Yang, Y.-W.; Wu, T.-Y.; Lue, J.-W.; Hsu, C.-H.; Sinha, S.; Mukherjee, M., *Langmuir* 2013, **29**, 3957-3967.
15. Hu, W.-S.; Weng, S.-Z.; Tao, Y.-T.; Liu, H.-J.; Lee, H.-Y., *Organic Electronics* 2008, **9**, 385-395.
16. (a) Huang, Z.; Geyer, N.; Werner, P.; de Boor, J.; Gösele, U., *Advanced Materials* 2011, **23**, 285-308; (b) Ho, C.-C.; Zhao, K.; Lee, T.-Y., *Nanoscale* 2014, **6**, 8606-8611.
17. Jurchescu, O. D.; Meetsma, A.; Palstra, T. T. M., *Acta Crystallographica Section B* 2006, **62**, 330-334.
18. Honglawan, A.; Beller, D. A.; Cavallaro, M.; Kamien, R. D.; Stebe, K. J.; Yang, S., *Advanced Materials* 2011, **23**, 5519-5523.
19. Kim, S. H.; Ahn, S. H.; Hirai, T., *Polymer* 2003, **44**, 5625-5634.
20. (a) Wu, K.-Y.; Tao, Y.-T.; Ho, C.-C.; Lee, W.-L.; Perng, T.-P., *Applied Physics Letters* 2011, **99**, 093306-3; (b) Johnston, D. E.; Yager, K. G.; Nam, C.-Y.; Ocko, B. M.; Black, C. T., *Nano Letters* 2012, **12**, 4181-4186; (c) Zan, H.-W.; Hsu, Y.-H.; Meng, H.-F.; Huang, C.-H.; Tao, Y.-T.; Tsai, W.-W., *Applied Physics Letters* 2012, **101**, 093307-4; (d) Fujimoto, K.; Hiroi, T.; Kudo, K.; Nakamura, M., *Advanced Materials* 2007, **19**, 525-530.
21. Austin, M. D.; Chou, S. Y., *Applied Physics Letters* 2002, **81**, 4431-4433.
22. Haddock, J. N.; Zhang, X.; Zheng, S.; Zhang, Q.; Marder, S. R.; Kippelen, B., *Organic Electronics* 2006, **7**, 45-54.
23. Reese, C.; Bao, Z., *Advanced Materials* 2007, **19**, 4535-4538.
24. A top-gate-top-contact device was made with the rubrene film prepared on nanopillar template, using parylene as gate dielectric and deposited Al as gate electrode. It should be noted that the conducting channel at the rubrene/parylene interface is not as smooth as that prepared on a flat substrate.